Characterization of the iridescence-causing multilayer structure of the *Ceroglossus suturalis* beetle using bio-inspired optimization strategies

Ana Luna,[1] Demetrio Macías,[2] Diana Skigin,[1,*] Marina Inchaussandague,[1] Daniel Schinca,[3] Miriam Gigli,[4] and Alexandre Vial[2]

[1]*Grupo de Electromagnetismo Aplicado, Departamento de Física, FCEN, Universidad de Buenos Aires, and IFIBA, CONICET Ciudad Universitaria, Pabellón I, C1428EHA Buenos Aires, Argentina*

[2]*Institut Charles Delaunay-Laboratoire de Nanotechnologie et d'Instrumentation Optique , (ICD-LNIO) UMR CNRS 6279, 12 rue Marie Curie - CS42060, FS-10004 Troyes CEDEX, France*

[3]*CIOp (CONICET, CIC), cc 124, 1900 La Plata, Argentina and Área Departamental de Ciencias Básicas, Facultad de Ingeniería, Universidad Nacional de La Plata, Argentina*

[4]*Departamento de Ciencias Exactas, Ciclo Básico Común, Universidad de Buenos Aires, Ciudad Universitaria, Pabellón III, C1428EHA Buenos Aires, Argentina*

**dcs@df.uba.ar*

Abstract: We investigate the iridescence exhibited by *Ceroglossus suturalis* beetles, which mostly live endemically in the southern end of South America. Two differently colored specimens have been studied. We observed and characterized the samples by different microscopy techniques, which revealed a multilayer structure within their cuticle. Using measured reflectance spectra as input data, we applied heuristic optimization techniques to estimate the refractive index values of the constituent materials, to be introduced within the theoretical model. The color of the samples was calculated for different incidence angles, showing that multilayer interference is the mechanism responsible for the observed iridescence.

OCIS codes: (170.1420) Biology; (230.4170) Multilayers; (050.1755) Computational electromagnetic methods; (330.1690) Color.

References and links

1. S. Kinoshita, *Structural Colors in the Realm of Nature* (World Scientific Publishing Co., 2008).
2. S. Berthier, *Iridescences, the Physical Colours of Insects* (Springer Science+Business Media, LLC, 2007).
3. S. M. Doucet and M. G. Meadows, "Iridescence: a functional perspective," J. R. Soc. Interface **6**, S115-S132 (2009).
4. S. Yoshioka and S. Kinoshita, "Single-scale spectroscopy of structurally colored butterflies: measurements of quantified reflectance and transmittance," J. Opt. Soc. Am. A **23**, 134–141 (2006).
5. W. Zhang, D. Zhang, T. Fan, J. Ding, J. Gu, Q. Guo, and H. Ogawa, "Biomimetic zinc oxide replica with structural color using butterfly (Ideopsis similis) wings as templates," Bioinsp. Biomim. **1**, 89-95 (2006).
6. R. J. Martín-Palma, C. G. Pantano, and A. Lakhtakia, "Biomimetization of butterfly wings by the conformal-evaporated-film-by rotation technique for photonics," Appl. Phys. Lett. **93**, 083901 (2008).
7. R. J. Martín-Palma and A. Lakhtakia, "Biomimetics and bioinspiration," Proc. SPIE **7401**, 1–196 (2009).

#191904 - $15.00 USD Received 6 Jun 2013; revised 12 Jul 2013; accepted 15 Jul 2013; published 6 Aug 2013

8. J.-P. Vigneron, M. Rassart, C. Vandenbem, V. Lousse, O. Deparis, L. P. Biró, D. Dedouaire, A. Cornet and P. Defrance, "Spectral filtering of visible light by the cuticle of metallic woodboring beetles and microfabrication of a matching bioinspired material," Phys. Rev. E **73**, 041905 (2006).
9. D. Mossakowski, "Reflection measurements used in the analysis of structural colours of beetles," J. Microsc. **116**, 351–364 (1979).
10. T. D. Schultz and M. A. Rankin, "The ultrastructure of the epicuticular interference reflectors of Tiger Beetles (Cicindela)," J. Exp. Biol. **117**, 87–110 (1985).
11. A. R. Parker, D. R. McKenzie and M. C. J. Large, "Multilayer reflectors in animals using green and gold beetles as contrasting examples," J. Exp. Biol. **201**, 1307–1313 (1998).
12. D. G. Stavenga, B. D. Wilts, H. L. Leertouwer and T. Hariyama, "Polarized iridescence of the multilayered elytra of the Japanese jewel beetle, *Chrysochroa fulgidissima*," Phil. Trans. R. Soc. B **366**, 709-723 (2011).
13. J. A. Noyes, P. Vukusic and I. R. Hooper, "Experimental method for reliably establishing the refractive index of buprestid beetle exocuticle," Opt. Express **15**, 4351–4357 (2007).
14. A. E. Seago, P. Brady, J.-P. Vigneron and T. D. Schultz, "Gold bugs and beyond: a review of iridescence and structural colour mechanisms in beetles (Coleoptera)," J. R. Soc. Interface **6**, S165-S184 (2009).
15. P. Yeh and A. Yariv, *Optical Waves in Crystals* (Wiley, 1984).
16. S. Yoshioka and S. Kinoshita, "Direct determination of the refractive index of natural multilayer systems," Phys. Rev. E **83**, 051917 (2011).
17. T. van de Kamp and H. Greven, "On the architechture of beetle elytra," Entomologie Heute **22**, 191–204 (2010).
18. H. M. Fox and G. Vevers, *The Nature of Animal Colours* (Sidgwick and Jackson, 1960).
19. P. Vukusic and D. G. Stavenga, "Physical methods for investigating structural colours in biological systems," J. R. Soc. Interface **6** S133–S148 (2009).
20. G. D. Bernard and W. H. Miller, "Interference filters in the corneas of Diptera," Invest. Ophtalmol. **7**, 416-434 (1968).
21. A. C. Neville, "Metallic gold and silver colours in some insect cuticles," J. Insect Physiol. **23**, 12671274 (1977).
22. H. Arwin, R. Magnusson, J. Landin and K. Jarrendahl, "Chirality-induced polarization effects in the cuticle of scarab beetles: 100 years after Michelson," Philos. Mag. **92**, 1583–1599 (2012).
23. D. Macías, A. Luna, D. Skigin, M. Inchaussandague, A. Vial, and D. Schinca, "Retrieval of relevant parameters of natural multilayer systems by means of bio-inspired optimization strategies," Appl. Opt. **52**, 2511–2520 (2013).
24. A. Luna, D. Skigin, M. Inchaussandague, and A. Roig Alsina, "Structural color in beetles of South America," Proc. SPIE **7782**, 778205 (2010).
25. B. Gralak, G. Tayeb, and S. Enoch. "Morpho butterflies wings color modeled with lamellar grating theory," Opt. Express **9**, 567-578 (2001).
26. R. Lozano, *El Color y su Medición* (Américalee Ed., 1978, in spanish).
27. The website EasyRGB http://www.easyrgb.com has the application Color calculator which converts color data to different color standars.
28. P. Henríquez, D. S. Donoso, and A. A. Grez, "Population density, sex ratio, body size and fluctuating asymmetry of *Ceroglossus chilensis* (Carabidae) in the fragmented Maulino forest and surrounding pine plantations," Acta Oecologica **35**, 811- 818 (2009).
29. *ImageJ* is a public domain, Java-based image processing program, http://rsbweb.nih.gov/ij/.

1. Introduction

Structural colors are widely spread in nature and generate different visual effects, such as iridescence and metallic appearance [1, 2]. Such colors have a physical origin and are produced by the interaction of light with the microstructures present in the cover tissues of biological organisms.

The diversity of structural color mechanisms and effects has attracted the attention of biologists, physicists and engineers [1, 2] not only due to the potential contribution to biological sciences by identifying the behavioural functions of the species [3], but also because natural structures might inspire biomimetic technologies for applications in different industries related to color [4–8].

Coleoptera display remarkable color effects generated by interference at the multilayer structures present at the external part of their cuticle [9–14]. The electromagnetic response of these species has been investigated by means of theoretical approaches based on planar multilayer systems. Although these theoretical calculations are simple and well known [15], the modelling of natural multilayer structures is still a challenging task as, usually, the top surface of the cuticle is corrugated and has a global curvature [16]. Also, the layers are not perfectly planar,

#191904 - $15.00 USD Received 6 Jun 2013; revised 12 Jul 2013; accepted 15 Jul 2013; published 6 Aug 2013

their thicknesses are not constant [12] and the structure varies from point to point of the sample [9, 16, 17]. Furthermore, the composition of the materials that constitute the layers depends on the species and it usually contains absorbing pigments [18]. Consequently, the refractive indices are not accurately known in most cases.

A precise knowledge of the constitutive parameters of the materials that compose biological tissues is essential for the study of natural multilayer systems [11, 19]. In earlier works, estimations of the refractive indices of the constituent materials were based on experimental reflectance measurements, by assuming ideal or non-ideal quater-wave stacks [9, 10, 20, 21]. More recently, different methods to establish the complex refractive indices of beetle's multilayer structures have been reported. Noyes *et al.* investigated the beetle *Chrysochroa raja* and found the complex refractive indices of the multilayer structure by fitting reflectance measurements for different angles and polarizations [13]. Yoshioka *et al.* [16] proposed an iterative procedure based on Cauchy's and Fresnel's equations to determine the complex refractive index of the jewel beetle from experimental data. Furthermore, Arwin *et al.* used Mueller matrix ellipsometry data to obtain the equivalent refractive index of the materials that constitute the multilayered cuticle of different beetles [22]. The refractive index values reported in the literature for the materials found in beetle's multilayers range between 1.4 and 2 for the real part and between 0 and 0.14 for the imaginary part.

In a fairly recent work, we explored the possibilities of heuristic optimization as a suitable tool to retrieve the dielectric constants of the multilayer structure that composes the cuticule of *Ceroglossus suturalis* beetles, a species that mostly lives endemically in the forest of the southern end of South America [23]. The preliminary results presented in that reference were quite promising and opened an alternative way for the solution of this kind of inverse problem.

In this contribution we investigate the mechanisms responsible for the metallic iridescent coloration of the *Ceroglossus suturalis*. The coloration of these beetles is of structural origin, and they appear with different hues, such as green, brown and blue. We study the response of green and brown samples, and calculate the observed color for different incidence angles [24]. In order to estimate the refractive indices of the materials comprising the multilayer structure, we apply the heuristic optimization techniques described in [23].

This work is structured as follows. In Sec. 2 we describe the samples and the methods used to characterize them via electron microscopy images. Also, we briefly summarize the multilayer model used to represent the electromagnetic response of the structure, the optimization strategies applied to estimate the refractive index values and we also explain the procedure to obtain the color from reflectance data. In Sec. 3 we show the results of the structural characterization of the analyzed samples of *Ceroglossus suturalis*. By introducing reflectance measurements data into the optimization algorithms, we estimate the layers' refractive indices. The color of the samples is calculated for different angles of incidence. Ultimately, in Sections 4 and 5 we discuss the results obtained and give our concluding remarks.

2. Materials and methods

2.1. Samples and characterization

We investigate the structural color generation in *Ceroglossus suturalis* beetles, that are Coleoptera and belong to the Carabidae family. They have a hard cuticle and can reach a length of 6 cm. Two types of samples of *Ceroglossus suturalis* were collected: the green samples are from Argentinean Patagonia, and the brown ones from the south of Chili (see Fig. 1).

The topography of the elytron (modified, hardened forewing) was observed with an Olympus SZ6045 stereoscopic microscope, and the images were captured with a digital camera. The samples were also observed with an Olympus BX60M Brightfield reflected light metallurgical microscope, and the images were captured by a Photometrics CoolSnap$_{cf}$ camera. The mi-

#191904 - $15.00 USD Received 6 Jun 2013; revised 12 Jul 2013; accepted 15 Jul 2013; published 6 Aug 2013

Fig. 1. Green and brown samples of *Ceroglossus suturalis* beetles under study.

crostructure of the elytron was characterized by a scanning electron microscope (SEM) Zeiss DSM 982 Gemini FESEM and a Zeiss Supra 40 FESEM, previous an Au sputtering treatment of 5 - 10 nm. Also, a transmission electron microscope (TEM) Philips-EM301 was used.

2.2. Measurements

The specular reflectance spectrum of the elytron was measured by using two optical fibers of 400 μm of diameter. One end of the first fiber was connected to a tungsten lamp, and the output beam was directed to the sample after being focused and linearly polarized. The light reflected by the sample was collected by the second fiber after passing through a Glan Thompson polarizer, and delivered to an Ocean Optics USB650 spectrometer (range 200 - 1100 nm, input slit 25 μm). The samples were mounted on a rotating plate that permitted the control of the incidence and reflection angles.

2.3. Electromagnetic model and optimization

In the case of the *Ceroglossus suturalis*, a multilayer structure is responsible for the iridescent effect. We employ the 4x4 transfer matrix method for one-dimensional multilayer systems [15, 24] to find the solution of the direct problem, i.e., to compute the scattered electromagnetic response given all the parameters of the structure (number of layers, refractive indices and thicknesses of the individual layers). Since the refractive indices of the biological tissues comprising the cuticle of the *Ceroglossus suturalis* are not precisely known, we estimate them by means of the inversion scheme described in [23], which couples the electromagnetic model with the heuristic optimization techniques and compares, along the inversion procedure, the numerically computed spectrum with the experimental one. For this, we make use of the functional

$$f(\mathbf{p}^T) = \|I^{\exp}(\lambda) - I^{\text{the}}(\lambda|\mathbf{p}^T)\|_2^2, \tag{1}$$

where $\|\|_2$ is the Euclidean Norm and the components of vector $\mathbf{p}^T$ are the parameters to be retrieved. Also, $I^{\exp}(\lambda)$ and $I^{\text{the}}(\lambda|\mathbf{p}^T)$ represent the experimentally measured and numerically generated spectra, respectively. The goal thus is to find a set of parameters that minimizes (1) and, if the solution is unique, reproduces the experimental optical signal $I^{\exp}(\lambda)$.

#191904 - $15.00 USD Received 6 Jun 2013; revised 12 Jul 2013; accepted 15 Jul 2013; published 6 Aug 2013

The three inversion schemes used in the present work are based on the bio-inspired population-based heuristic optimization techniques described in [23] and references therein: Evolution Strategies, in their Elitist (EL) and Non-Elitist (NE) variants, and Particle Swarm Optimization (PSO).

2.4. Color calculation

The concept of color can be divided into two parts: brightness and chromaticity. In 1931, the International Commission on Illumination (CIE) defined three standard primaries, the CIE X, Y, and Z tristimulus values. The corresponding functions $\overline{x}$, $\overline{y}$ and $\overline{z}$ are called color-matching functions and describe the chromatic response of the observer. The $\overline{y}$ color-matching function is defined to match the eyes sensitivity to brightness; the other two do not correlate with any perceptual attibutes. X, Y and Z represent the weights of the respective color-matching functions needed to approximate a particular spectrum [25].

Let us consider that the structure under study has a reflectivity $R(\lambda)$ when illuminated by an illuminant characterized by its energy distribution $D(\lambda)$. Following the CIE definitions, the three standard tristimulus values X, Y, and Z can be calculated [25]:

$$\begin{aligned} X &= \frac{1}{k}\int D(\lambda)R(\lambda)\overline{x}(\lambda)\,d\lambda\,, \\ Y &= \frac{1}{k}\int D(\lambda)R(\lambda)\overline{y}(\lambda)\,d\lambda\,, \\ Z &= \frac{1}{k}\int D(\lambda)R(\lambda)\overline{z}(\lambda)\,d\lambda\,. \end{aligned} \tag{2}$$

In eq. (2) k is a normalization factor defined in such a way that an object with a uniform reflectivity $R(\lambda) = 1$ gives a luminance component Y equal to 1. To analyze the color observed by the human eye, it is sufficient to retain in the integrals of eq. (2) only the wavelengths within the visible range (380 - 780 nm). To visualize the colors in the screen, the XYZ components are converted into RGB components through a linear transformation [26, 27]. The chromaticity of a color can be specified by the two normalized parameters x and y, which depend on the three tristimulus values X, Y, and Z:

$$\begin{aligned} x &= \frac{X}{X+Y+Z}\,, \\ y &= \frac{Y}{X+Y+Z}\,. \end{aligned} \tag{3}$$

The chromaticity diagram is a 2D plot and in this paper we use this kind of diagram to illustrate the color variation with the relevant parameters of the model.

3. Results

3.1. Color observation

In Fig. 1 we show a photo of the two samples of *Ceroglossus suturalis* under investigation. The elytra of these beetles display an iridescent green or brown color, depending on the sample. In both cases, the elytron exhibits ridges, and in the green specimen also short brownish segments are observed. There are no differences in coloration between male and female individuals [28]. Observing the elytron at increasing magnifications reveals that the color of the surface is not uniform and varies between yellow and violet for both kinds of samples, as already reported for other beetles (see Fig. 2) [12]. This suggests that the multilayer structure responsible for the iridescence can have local variations in thickness and in refractive index. When changing

#191904 - $15.00 USD Received 6 Jun 2013; revised 12 Jul 2013; accepted 15 Jul 2013; published 6 Aug 2013

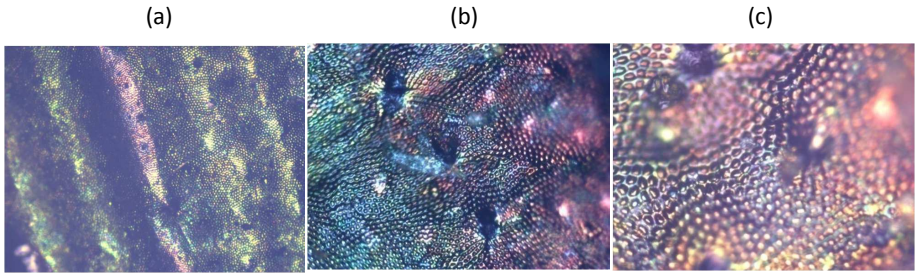

Fig. 2. Images of the elytron topography observed with an optical microscope with different magnifications: (a) 50X; (b) 100X; (c) 200X.

the viewing angle from normal to oblique, both samples smoothly change their coloration. This iridescent feature constitutes an evidence of the structural origin of the color of *Ceroglossus suturalis* beetles.

3.2. Structural characterization

As already observed in Fig. 2 for the green sample, the top surface of the elytron is covered with alveoli or micro-protuberances of $\approx 10\ \mu$m diameter, and a height of $\approx 2.5\ \mu$m. This is a common feature of both specimens, as observed in Fig. 3 for the brown beetle. These corrugations scatter light and produce an angular widening of the reflected peak, which also affects the observed color [13]. Since the radius of curvature of the bumps is rather large compared with visible wavelengths, we can assume that, in a first order approximation, the elytron acts as a planar reflector.

The structural arrangement that produces color in this species is a multilayer structure composed of alternating layers of different optical densities, located in the epicuticle. SEM images of the green beetle's elytron cross-section are shown in Fig. 4 with different magnifications. The structure of the epicuticle inside the elytron consists of a periodic multilayer, where each period is a bi-layer of materials with different optical densities [24]. It is important to remark that the multilayer structure varies from point to point [17], and then each image is not representative of the complete system but only of a very localized area. An average of 9 periods was found in the images of Fig. 4. Also, the thicknesses of the layers where about 100 nm and 60 nm and make a total average thickness of $\approx 1.4\ \mu$m. The brown beetle's elytron has a completely similar structure; in this case the multilayer consists of 20 periods, and the thicknesses of the layers are about 120 nm and 70 nm (the total average thickness of the multilayer is $\approx 3.8\ \mu$m). The relevant geometrical parameters were obtained after an exhaustive study and analysis of the SEM and TEM images using the *ImageJ* software [29]. The extraction of parameters was completed with a statistical analysis.

3.3. Measurements

In Fig. 5 we show the experimental reflectance curves obtained for both samples using the setup explained in Sec. 2.2, for an incidence angle of 30° and TE polarization. A typical response of beetle's elytra is observed: for the green sample [Fig. 5(a)] the reflectance peak is located at ≈ 560 nm, whereas for the brown one [Fig. 5(b)] the maximum is at ≈ 610 nm. In both cases, the peak width is ≈ 100 nm, as already observed for other species in this kind of measurements [8, 9, 12, 13]. The measured reflectance curves displayed in Fig. 5 will play the role of target

#191904 - $15.00 USD Received 6 Jun 2013; revised 12 Jul 2013; accepted 15 Jul 2013; published 6 Aug 2013

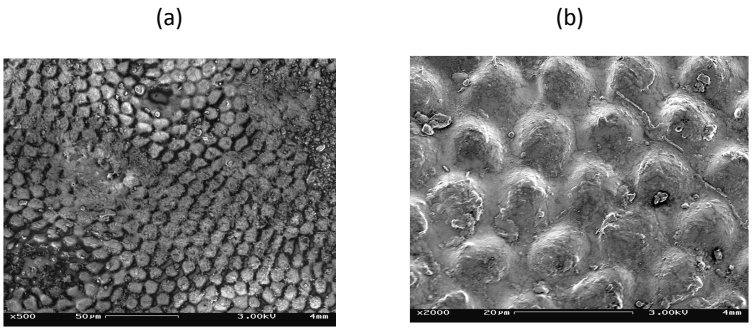

Fig. 3. SEM images of the elytron topography of a metalized sample of the brown specimen, with different magnifications.

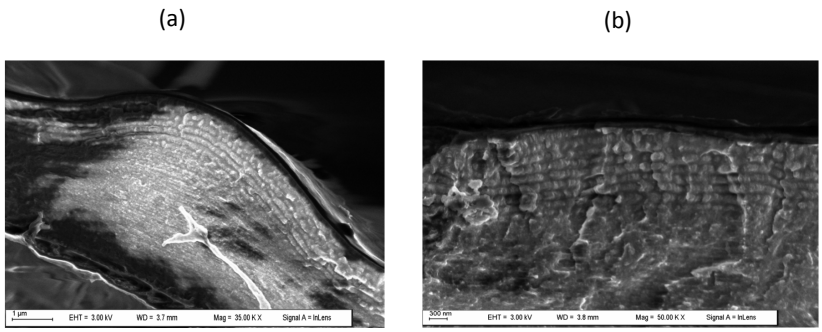

Fig. 4. SEM images of a transversal cut of the elytron of a green sample, with different magnifications.

functions for the retrieval scheme proposed to estimate the refractive indices and the thicknesses of the layers.

3.4. Estimation of the refractive indices

In order to calculate the electromagnetic response of the structure using the 4x4 approach, the refractive indices of the layers must be introduced. As mentioned above, the determination of the dielectric constant of biological tissues constitutes a challenge in itself, and different approaches had been proposed. In this work we apply optimization strategies to obtain the refractive indices from experimental data. For this purpose, we propose two different numerical experiments. In the first one, we restrict the search to the real and imaginary parts of the two materials that constitute the multilayer, i.e., we will look for four unknown variables and the values of the thicknesses are taken from the analyzed images. Since the thicknesses strongly depend on the observed sample and also vary along the elytron, in the second study we will

#191904 - $15.00 USD Received 6 Jun 2013; revised 12 Jul 2013; accepted 15 Jul 2013; published 6 Aug 2013

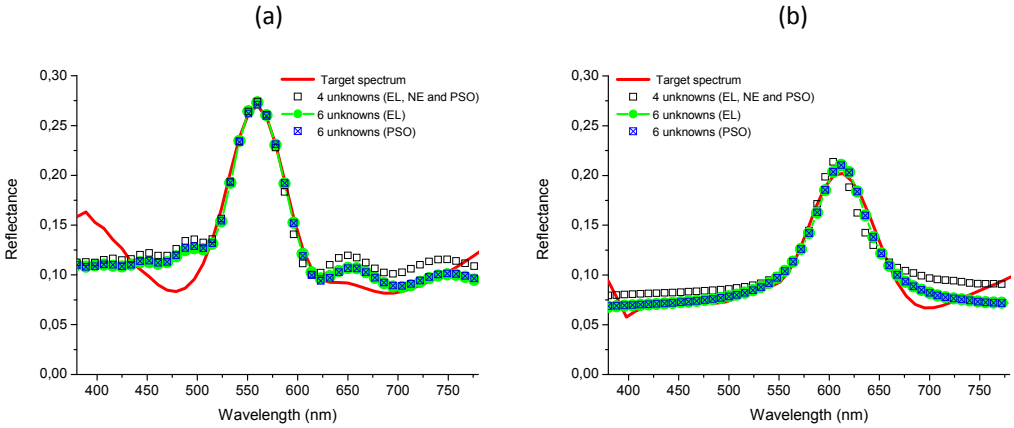

Fig. 5. Reflectance spectra for an incidence angle of 30° and TE polarization. The experimental curve is shown in solid red line, and the different optimized curves obtained via the heuristic strategies are also shown. (a) Green sample; (b) brown sample.

also include the thicknesses as variables to be determined, making a total of six unknowns. In what follows we describe the results obtained.

3.4.1. First experiment: fixed layers' thicknesses (four unknowns)

In order to retrieve the complex dielectric constants of the materials that comprise this natural system, we assumed a perfectly periodic planar multilayer structure with known values of the layers' thicknesses, taken from the analyzed images. In the case of the green sample we have $d_1 = 60$ nm and $d_2 = 100$ nm, and for the brown one $d_1 = 70$ nm and $d_2 = 120$ nm. The total number of periods –each comprising two different layers– was also fixed to 9 for the green beetle and to 20 for the brown one. The dielectric constant of the substrate is assumed to be the average of those of the individual layers, as reported for other beetles' structures [12].

We employed our in-home implementations of the three schemes described in [23]. In what concerns the elitist and non-elitist evolution strategies (EL and NE), we set the size of the initial and the secondary populations to 14 and 100, respectively, and we fixed the number of elements to be recombined to 2. The number of initial states from where we searched for the optimum (realizations) was set to 200 and the number of generations in each evolutionary loop was set to 200 and it provided the termination criterion. Each element of the population was a set of randomly generated values of the complex dielectric constants ε_1 and ε_2. In order to compare the PSO with the EL and the NE in an objective manner, we set the size of the swarm to 114. We considered the same number of iterations for the optimization loop so that the fitness function was evaluated by the PSO the same number of times as in the EL and the NE schemes. To define the search space, in all cases we set the lower and upper bounds $0 \leq \Re\{\varepsilon_1\}, \Re\{\varepsilon_2\} \leq 5$, $0 \leq \Im\{\varepsilon_1\}, \Im\{\varepsilon_2\} \leq 1$, which correspond to reasonable ranges for the dielectric constants found in natural tissues. We considered as target curve the reflectance for an incidence angle of 30° and TE polarization, restricted to the visible range, i.e., to wavelengths between 380 and 780 nm.

In the search for the optimized solution for the green specimen, 100% of the realizations of the EL and the PSO converged to the values $n_1 = 1.78 + i\,0.07$ and $n_2 = 1.85 + i\,0.02$, with a fitness of ≈ 0.21. However, the NE converged to this solution only in the 74% of the realizations. An 8% of the realizations converged to another set of refractive indices, which was discarded

#191904 - $15.00 USD Received 6 Jun 2013; revised 12 Jul 2013; accepted 15 Jul 2013; published 6 Aug 2013

for having some of the values out of the bounds of the search space, and this suggests that they do not correpond to a global optimum but to a local one. The rest of the solutions (18%) gave extremely high values of the fitness function, meaning that they do not correspond to optimized solutions. According to these results, the EL and the PSO appear as more successful strategies in comparison with the NE, for this particular example. The calculated reflectance spectrum obtained with the optimized values is depicted in Fig. 5(a). It can be observed that the location, amplitude, width and shape of the peak are very well matched with the experimental curve (solid line). The most significant differences appear at both sides of the peak. Althought the optimized values of the refractive indices are contained within the expected values for natural tissues present in the beetle's cuticle multilayers [2], their real parts appear rather high, if we compare them with similar species such as the *Chrysochroa raja*, for which values of 1.55 and 1.68 were reported [13], or the *Chrysochroa fulgidissima*, whose values range between 1.65 and 1.8 for the high index and between 1.55 and 1.6 for the low index, as reported in [16]. On the other hand, the retrieved imaginary parts lie very well within the reported ranges for beetles' multilayers.

For the brown sample, the EL converged to the following values for all the realizations: $n_1 = 1.61 + i\ 0.07$ and $n_2 = 1.69 + i\ 0.05$, with a fitness of 0.08. The PSO gave the same solution in 88% of the realizations, and the NE only in 74%. The rest of the solutions found by the PSO (12%) correspond to another set of values, which has a slightly higher fitness (0.09): $n_1 = 1.78 + i\,0.03$ and $n_2 = 1.43 + i\,0.08$, which suggests that this solution might correspond to a local optimum. In the case of the NE, the rest of the realizations did not converge to acceptable solutions from the point of view of the fitness value. Therefore, also in this case the EL and the PSO appear as more succesful strategies than the NE. The calculated reflectance curve using the retrieved values of the refractive indices is shown in Fig. 5(b). Also in this case, the main features of the experimental reflectance (solid curve) are very well reproduced by the optimized curve. These refractive index values are also contained within the reported ranges for similar species.

3.4.2. Second experiment: variable layers' thicknesses (six unknowns)

Although the refractive index values retrieved in the previous subsection are acceptable from the point of view of biological tissues present in the beetles' cuticle, the optimized curves and the target spectra do not fully overlap, and this suggests that a more realistic set of solutions could be obtained. In order to improve these estimations, in this subsection we enlarge the unknowns' domain up to six, i.e., we also include the thicknesses of both layers as unknown variables to be retrieved. It is well known that the layers' thicknesses vary from one sample to the other, and even in different regions within the same sample, and we cannot certainly know the thicknesses underlying the illuminated spot [12]. Therefore, the inclusion of the thicknesses as unknown variables appears as a natural way of improving the search for the actual values of the refractive index.

Taking into account that the EL and the PSO seem to be more successful than the NE in retrieving the refractive indices in the case of four unknowns, we restrict this extended study to those strategies. For these calculations the number of initial states (realizations) was set to 50, and the rest of the parameters were the same as those used in the preceding subsection except the layers' thicknesses, which are variable.

The substantial difference between the results obtained for four and for six unknowns is that in this last case, both inversion schemes give different solutions for each one of the realizations considered, i.e., all the sets of six retrieved values are essentially different from each other. Therefore, each one of the solutions sets have different values of the fitness function. As the number of unknowns is increased, the topology of the fitness function becomes more complex,

#191904 - $15.00 USD Received 6 Jun 2013; revised 12 Jul 2013; accepted 15 Jul 2013; published 6 Aug 2013

and this produces a higher probability of the algorithms to converge to a local optimum (apparent, nondesired solution) instead of the global one (target solution). Therefore, since in the proposed inversion schemes the measure of the closeness to the target values is given via the functional of eq. (1), the set of values that minimizes the fitness appears to be the best candidate for the searched parameters.

In Table 1 we show the best sets of variables (Real and Imaginary parts of the refractive indices and both thicknesses) obtained for the green and the brown samples using the EL and the PSO strategies, as well as the corresponding values of the fitness function (f). To facilitate the comparison, we also include in the table the refraction index retrieved considering only four unknowns (Sec. 3.4.1).

Table 1. Retrieved values of the Real and Imaginary parts of the refraction indices and of the layers' thicknesses (d_1 and d_2), and the corresponding fitness values using the EL and the PSO, for the green and brown samples.

	Green sample			Brown sample		
	EL (6v)	PSO (6v)	EL/PSO (4v)	EL (6v)	PSO (6v)	EL/PSO (4v)
$\Re\{n_1\}$	1.654	1.679	1.78	1.510	1.507	1.61
$\Im\{n_1\}$	0.028	0.037	0.07	0.071	0.068	0.07
$\Re\{n_2\}$	1.777	1.781	1.85	1.606	1.604	1.69
$\Im\{n_2\}$	0.119	0.060	0.02	0.059	0.061	0.05
d_1 (nm)	139.30	115.51	–	98.87	102.04	–
d_2 (nm)	36.50	56.74	–	108.10	105.49	–
f	0.154	0.158	0.21	0.031	0.031	0.08

The first indication that the new solutions are better than the previous ones, is the decrease of the fitness function. In all cases the value of f is diminished compared with the four variables case, and this confirms that the target reflectance is better reproduced by our planar multilayer model for the new retrieved sets of values. Another encouraging result is that the best sets obtained via the EL and the PSO, which are completely different and independent strategies, give very similar values of refractive indices. The fact that both schemes converge to close results gives more confidence to the solutions, and suggests that they are suitable for this task. Also, it can be noticed that the real parts of the refractive indices are lower than those obtained with four unknowns, and then, they are closer to the recently reported refractive index values of similar biological systems [13, 16]. Consequently, the retrieved values of the thickness seem to approach better to the actual values involved in the reflectance measurement sample (illuminated spot) than those used in the first experiment (fixed values obtained from different microscopy images). This also evidences that the thickness values used in the retrieval of four unknowns strongly condition the retrieved refraction index values, and then, the six unknowns experiment appears to be more suitable for dealing with this multilayer structure. Taking into account that we considered 9 periods for the green beetle, the obtained total thickness of the multilayer is 1582,20 nm for the EL and 1550.25 nm for the PSO. For the brown beetle (20 periods), we obtained a total thickness of 4139.4 nm for the EL and 4150.6 nm for the PSO. These values are slightly larger than the average values measured from the SEM images (Sec. 3.2). This result is to expect since, as mentioned above, the layers' thicknesses vary from one sample to the other and even in different regions of the same sample. In Fig. 5 we also plot the calculated reflectance obtained with the refractive indices retrieved with the six unknowns experiment for the green [Fig. 5(a)] and the brown [Fig. 5(b)] samples. It is evident that the obtained curves constitute a better approach to the target ones.

#191904 - $15.00 USD Received 6 Jun 2013; revised 12 Jul 2013; accepted 15 Jul 2013; published 6 Aug 2013

This result suggests that the use of optimization strategies such as the EL and the PSO for the retrieval of the refractive indices of biological structures is a critical task that should be carefully carried out, and in the case of multilayer structures the inclusion of the layers' thicknesses as unknowns significantly improves the quality of the solution. Although the refraction indices estimated with the six unknowns experiment lie within the reported values of the cuticle components of beetles, the obtained values are still rather high if compared with those obtained by other authors for similar beetles [12, 13, 16]. It is important to mention that the electromagnetic model used within the retrieval algorithms could be further improved by including other characteristics of the actual natural system, such as surface roughness, curvature, and the inhomogeneity in the thicknesses of the layers along the multilayer stack. Better estimations of the refraction indices could also be obtained by including the refraction index of the substrate as another unknown to be retrieved.

In order to explore the behaviour of the retrieved set of values, in Fig. 6 we plot the calculated reflectance and absorptance as a function of the wavelength for different angles of incidence and for both samples considered. As expected, the reflectance peak shifts to shorter wavelengths as the incidence angle increases and also the overall reflectance increases. The reflectance peak is smoother for the brown than for the green sample and this behaviour has already been reported in similar beetles having green and purple regions in their elytra [12].

3.5. Color calculation

As stated above, *Ceroglossus suturalis* beetles exhibit iridescent color, i.e., the observed hue changes as the angle of observation moves from normal to grazing. It is interesting then to investigate if the retrieved parameters account for such phenomenon. Taking into account the reflectance spectra of Figs. 6(a)-6(b), we calculated the chromaticity coordinates obtained as described in Sec. 2.4, for a CIE standard illuminant A and for a visual field of 10°. In Fig. 7 these coordinates are plot in chromaticity diagrams for each sample, for several incidence angles. It can be observed that as the incidence angle increases, the color position in the diagram describes a curved path in the anticlockwise direction, and this occurs for both samples. However, in the green specimen case, the color reaches the greens' zone of the diagram, whereas for the brown sample it always remains within the brown-orange region. Notice that the chromaticity diagram is a 2D plot where it is not possible to represent the actual brightness of the color, which should be accounted for by the z coordinate (not shown).

Using the x and y chromaticity coordinates given by eq. (3), we obtained the corresponding RGB coordinates which permit visualizing the sequence of colors for each beetle, when the angle of incidence is varied. The results are shown as squares below each one of the chromaticity diagrams. It is evident that the color changes with the incidence angle for both samples. The green beetle exhibits a green hue up to 50°, and then it becomes orange. The brown sample also preserves the brown coloration to an incidence angle of 50°.

4. Discussion

The multilayered cuticle of Coleoptera is one of the simplest examples of natural photonic crystals. However, a precise characterization of such structures is extremely difficult. From one hand, the layers' thicknesses vary between samples and even within different sections of the same sample. From the other hand, highly precise cuts must precede the electron microscopy images from which the layers' thicknesses are obtained. Since the sample section used for the reflectance measurement is always different from the samples imaged by electron microscopy, there is an uncertainty regarding the actual parameters that correspond to the reflectance curve. On top of that, the roughness and curvature that exhibit these kind of samples make it extremely difficult to make reliable reflectance measurements, and then, the measurement constitutes a

#191904 - $15.00 USD Received 6 Jun 2013; revised 12 Jul 2013; accepted 15 Jul 2013; published 6 Aug 2013

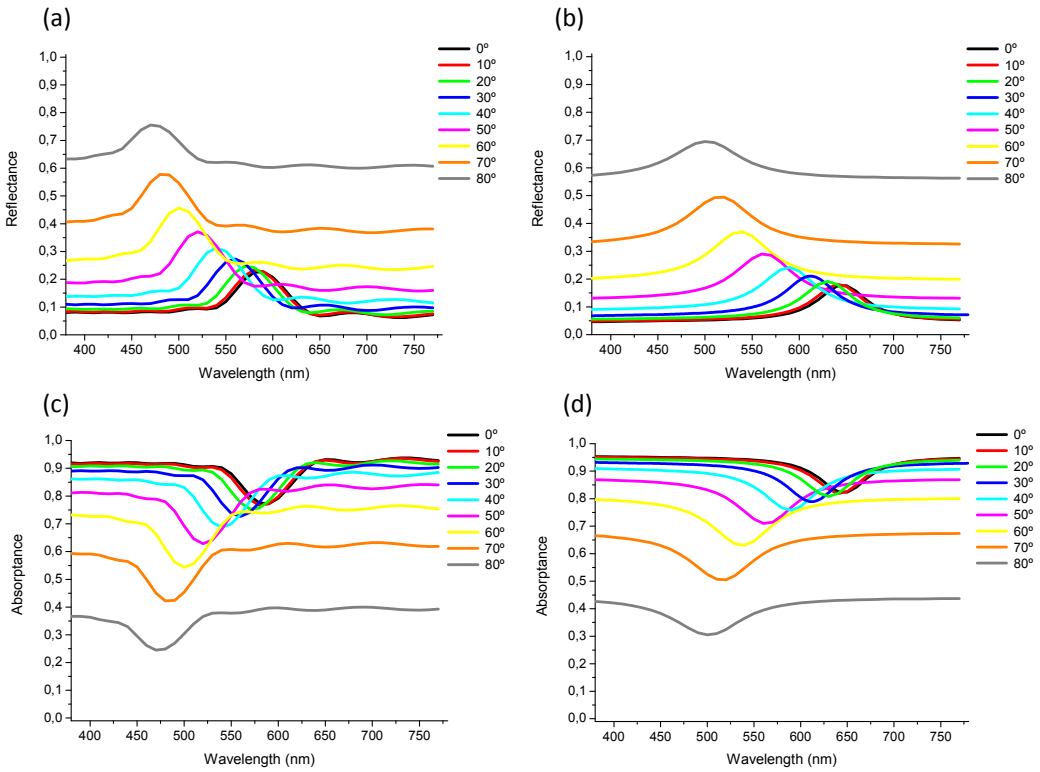

Fig. 6. Reflectance and absorptance spectra for different angles of incidence and TE polarization. (a) Reflectance for the green sample; (b) Reflectance for the brown sample; (c) Absorptance for the green sample; (d) Absorptance for the brown sample.

challenge in itself.

Another critical issue is the degree of proximity of the natural system to the ideal model proposed to reproduce its response. In the present example, we considered a perfectly periodic planar multilayer structure as a model for the actual system. Therefore, it is important to remark that the electromagnetic model used within the retrieval algorithms could be further improved by including other characteristics of the actual natural system, such as surface roughness, curvature, and the inhomogeneity in the thicknesses of the layers along the multilayer stack. Better estimations of the refraction indices could also be obtained by including the refraction index of the substrate as another unknown to be retrieved. The sensitivity of the retrieved values to the assumptions involved in the model is expected to decrease as the description of the real system becomes more accurate. Also, in the present case we assumed that the materials which comprise the layers are characterized by isotropic non-dispersive dielectric permittivities. However, it is well known that the cuticle of many Coleoptera exhibit anisotropy in their constituent materials [22], and also dispersion has been reported [16]. Therefore, one way to improve the estimation of the retrieved parameters would be to consider anisotropic and dispersive materials for the layers. Besides, the layers' thicknesses distribution is not perfectly periodic [13], and then, to relax the perfect periodicity assumption would also contribute to a better representation of the natural system, which, in turn, would result in a more accurate estimation of the unknown parameters.

#191904 - $15.00 USD Received 6 Jun 2013; revised 12 Jul 2013; accepted 15 Jul 2013; published 6 Aug 2013

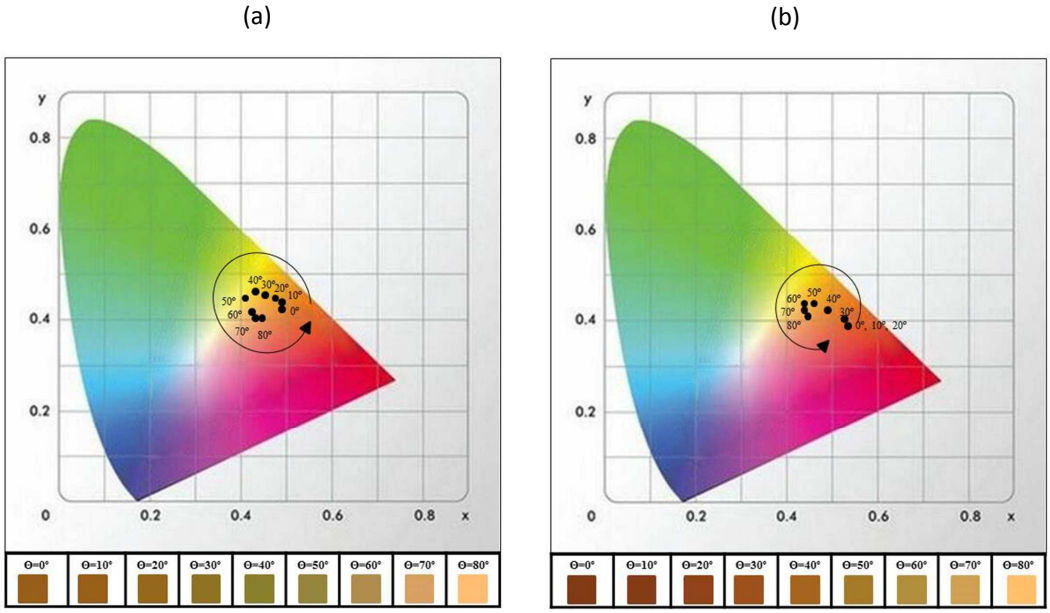

Fig. 7. Color coordinates of the beetles samples for different incidence angles. (a) Green sample; (b) brown sample.

5. Conclusions

We investigated the structural color generation in *Ceroglossus suturalis* beetles. Two differently colored samples have been analyzed and characterized by different microscopy techniques, which revealed a multilayered structure within the specimen's cuticle. A careful measurement of their reflectance spectra has been done, and this allowed the estimation of the complex values of the refractive indices using optimization strategies. The obtained values were introduced in the planar multilayer model to compute the electromagnetic response of the structure. The observed color was calculated for different angles of incidence, and this confirms that multilayer interference is the underlying mechanism responsible for the observed iridescence.

Acknowledgments

We thank Dr. A. Roig Alsina for supplying the beetles' specimens used in this study. A. L., D. S. and M. I. acknowledge partial support from Consejo Nacional de Investigaciones Científicas y Técnicas (CONICET PIP 112-200801-01880) and Universidad de Buenos Aires (UBA-20020100100533).

#191904 - $15.00 USD Received 6 Jun 2013; revised 12 Jul 2013; accepted 15 Jul 2013; published 6 Aug 2013